

This Page Is Inserted by IFW Operations  
and is not a part of the Official Record

## **BEST AVAILABLE IMAGES**

Defective images within this document are accurate representations of the original documents submitted by the applicant.

Defects in the images may include (but are not limited to):

- BLACK BORDERS
- TEXT CUT OFF AT TOP, BOTTOM OR SIDES
- FADED TEXT
- ILLEGIBLE TEXT
- SKEWED/SLANTED IMAGES
- COLORED PHOTOS
- BLACK OR VERY BLACK AND WHITE DARK PHOTOS
- GRAY SCALE DOCUMENTS

**IMAGES ARE BEST AVAILABLE COPY.**

**As rescanning documents *will not* correct images,  
please do not report the images to the  
Image Problems Mailbox.**

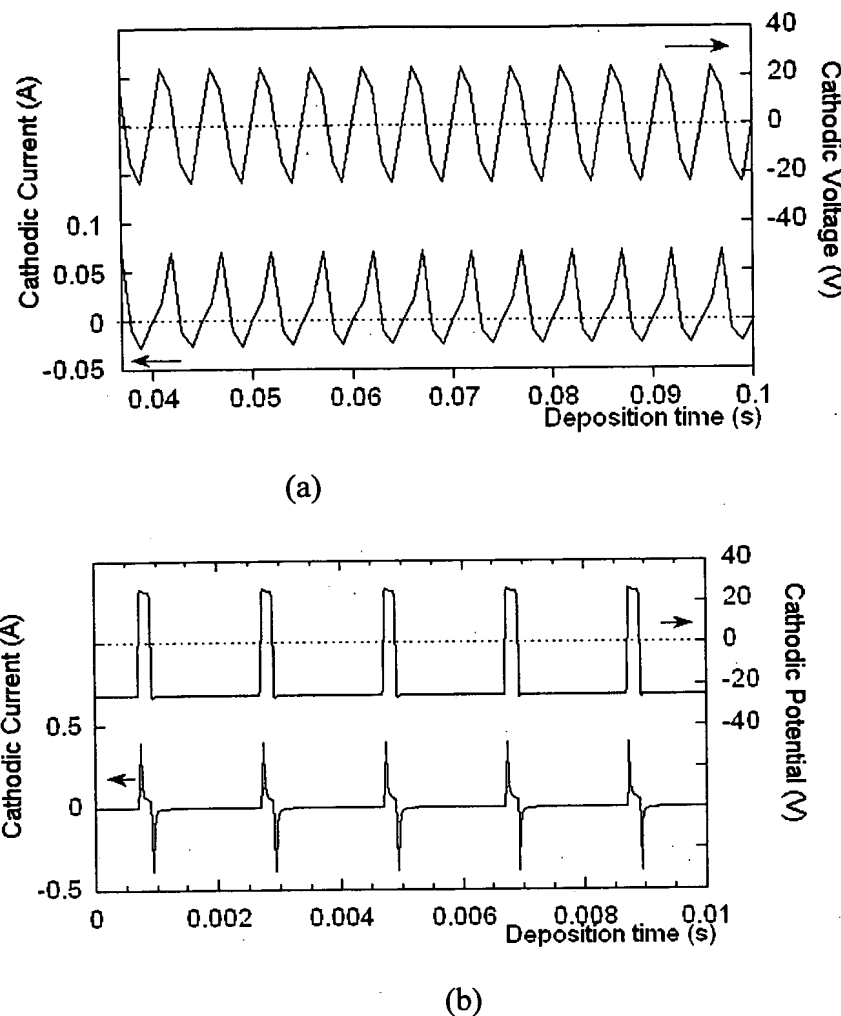


Fig. 1. Two examples of voltage waveforms and resulting current transients employed in the electrodeposition of Co arrays. (a) Sinusoidal AC waveform, (b) Asymmetric rectangular waveform.

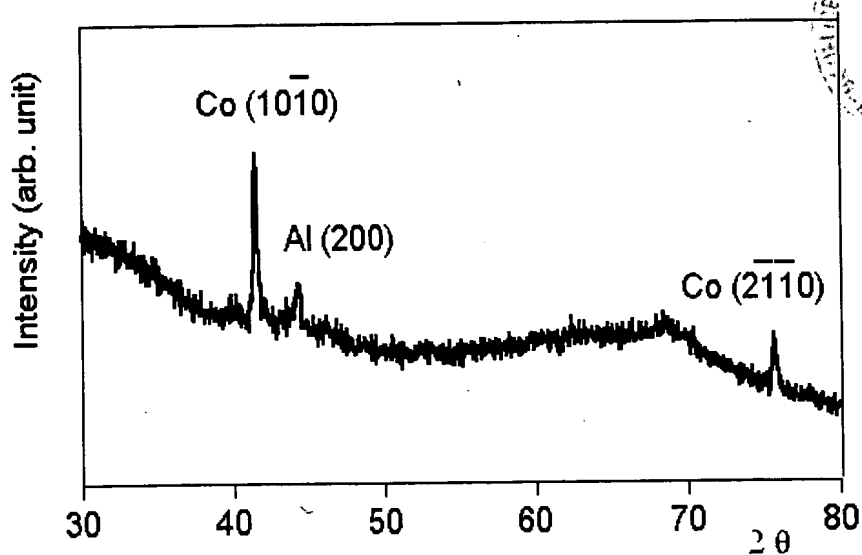


Fig. 2. XRD diffractogram of the Co-filled alumite film. A sinusoidal waveform was used for electrodeposition. Particle length = 1  $\mu\text{m}$ , particle diameter = 5 nm.

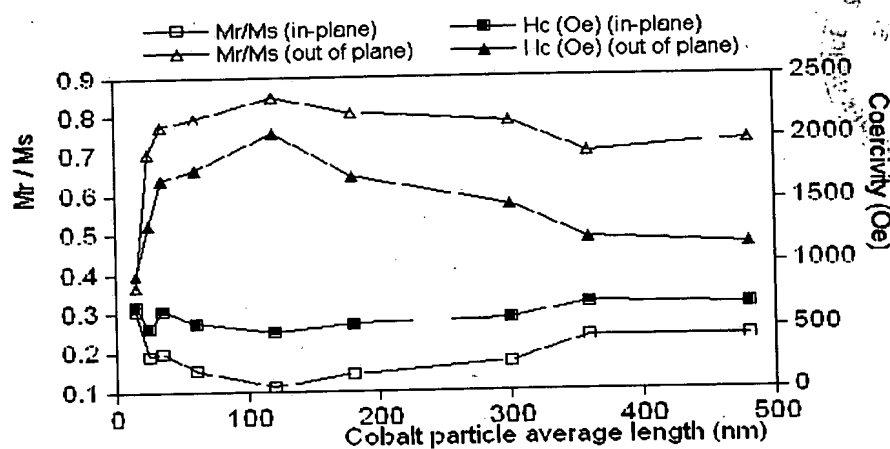


Fig. 3. In-plane and perpendicular squareness  $S = M_r / M_s$  and coercivity vs. nanowire length  $l$  for Co arrays grown using a sinusoidal waveform.

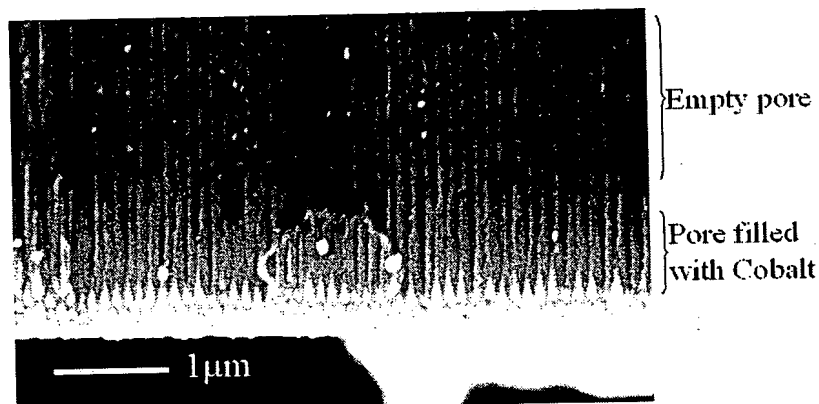


Fig. 4. Cross-sectional SEM image of a Co-filled alumite sample grown using a sinusoidal waveform. Co nanowires are bright in the figure. Mean nanowire length  $l = 1.2$  μm, diameter = 25 nm.

5

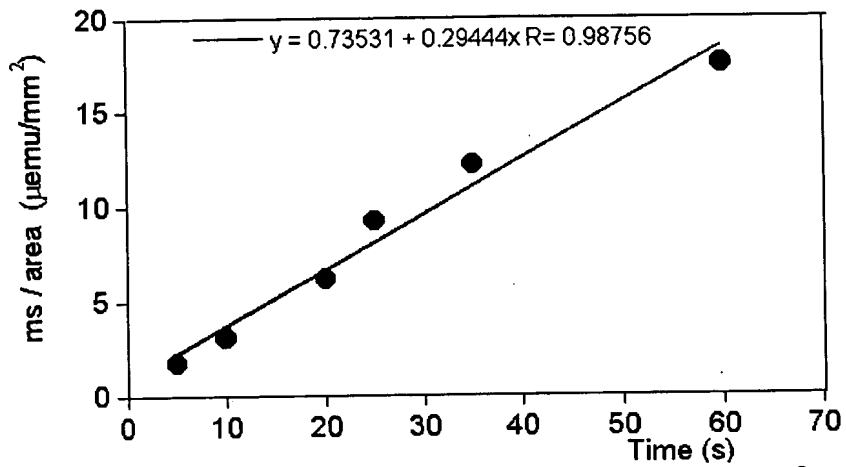
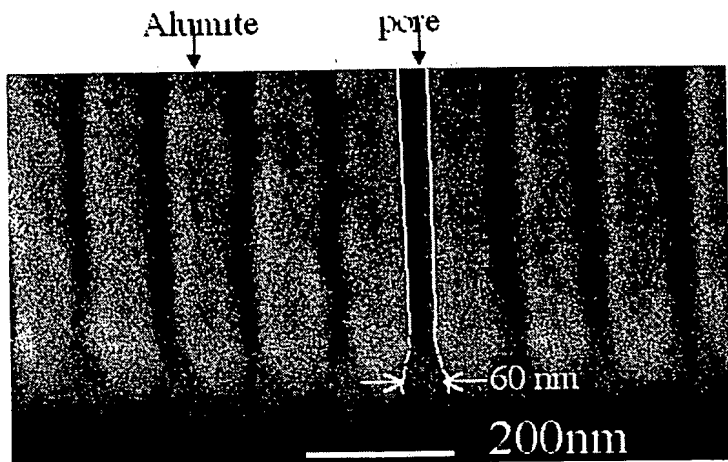
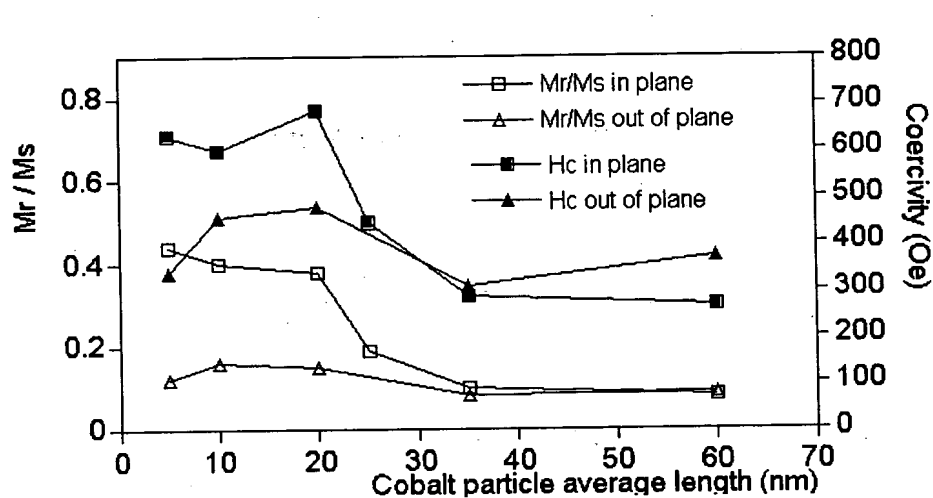


Fig. 5. Electrodeposition rate when using the asymmetric waveform of Fig. 1b. (saturation magnetization  $m_s$  per unit area, as a function of electrodeposition time  $t$ ).



5 Fig. 6. SEM Cross-section of alumite pores (no Co in the pores) after anodization in phosphoric acid – the pore widening to  $d = 60$  nm diameter is highlighted in the center.



15 Fig. 7. In-plane and out-of-plane coercivity  $H_c$  and squareness  $M_r / M_s$  vs. average nanoparticle length  $l$ : a transition is seen for  $l < 20$  nm.

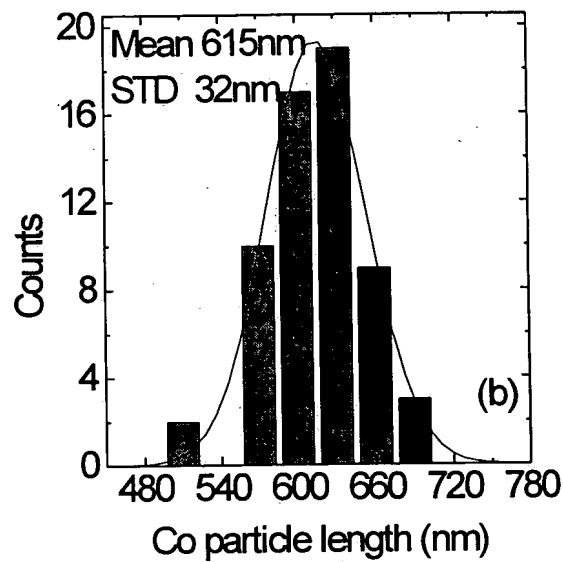
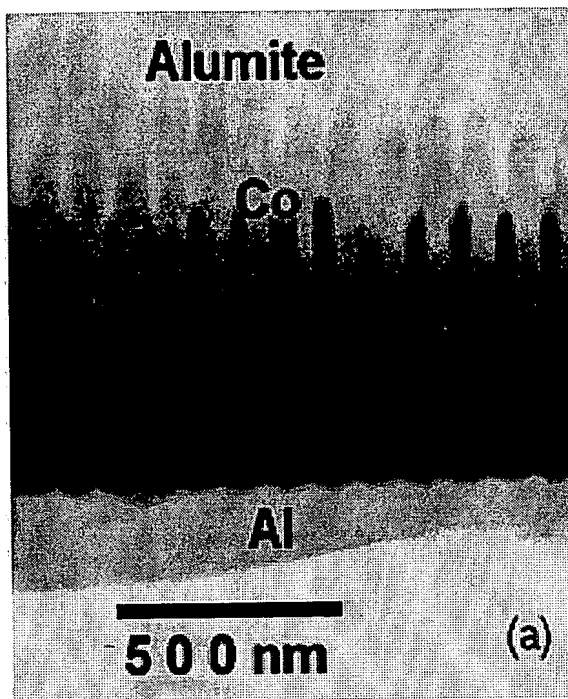


FIG. 8 (a) TEM cross-sectional view of Co arrays in alumite with average length 615 nm. (b) Length distribution determined over 60 particles.

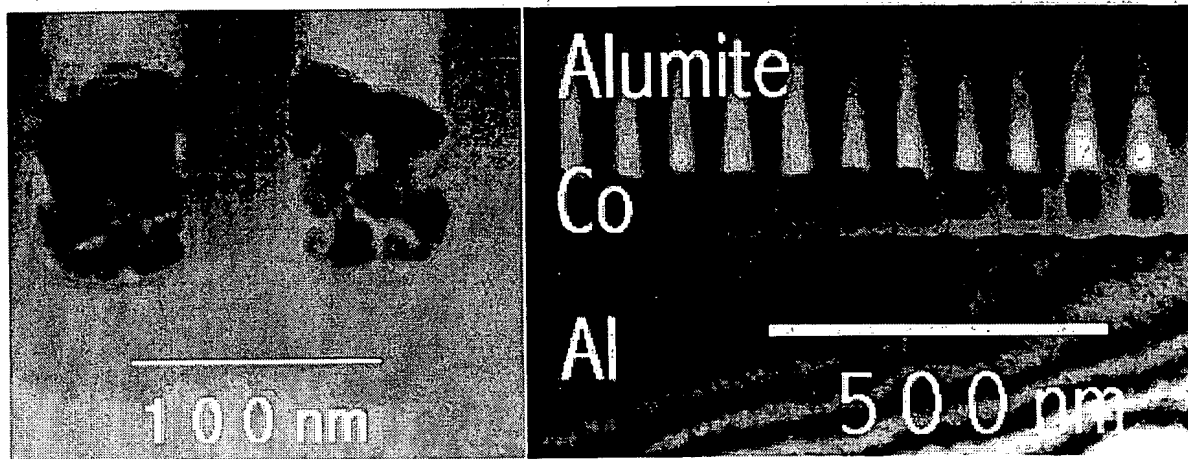
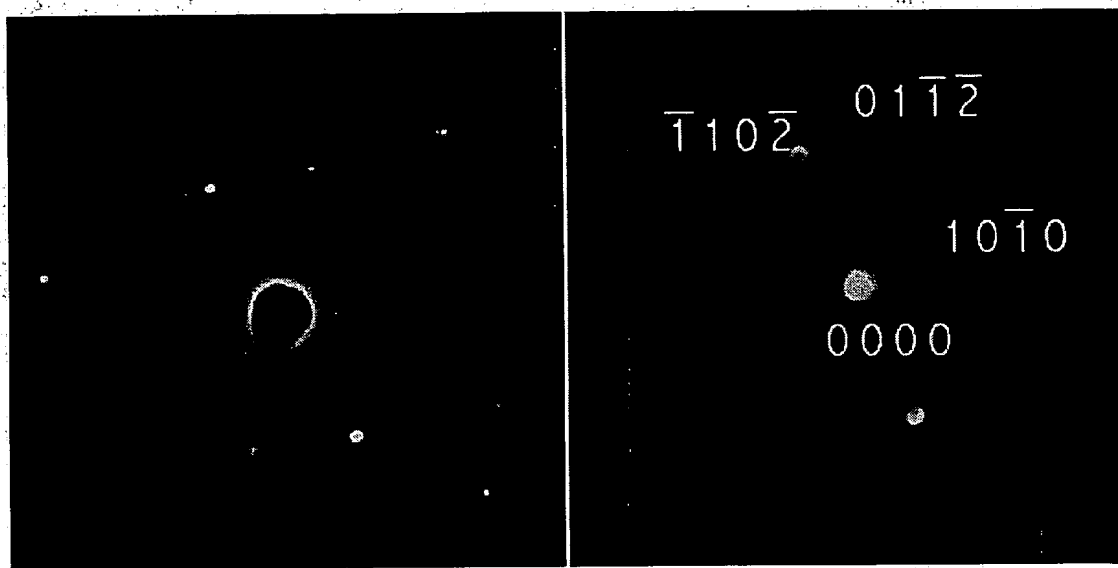


FIG. 9 TEM cross section of Co particles in ordered alumite. Left: details of the microstructure. Right: overview, showing the thickness uniformity.



5 FIG. 10 TEM selected area diffraction patterns of (left) several grains of one Co particle, showing HCP ring patterns superposed to Al (112), and (right) the Co HCP ( $\underline{2}4\underline{2}3$ ) diffraction pattern corresponding to one large grain.

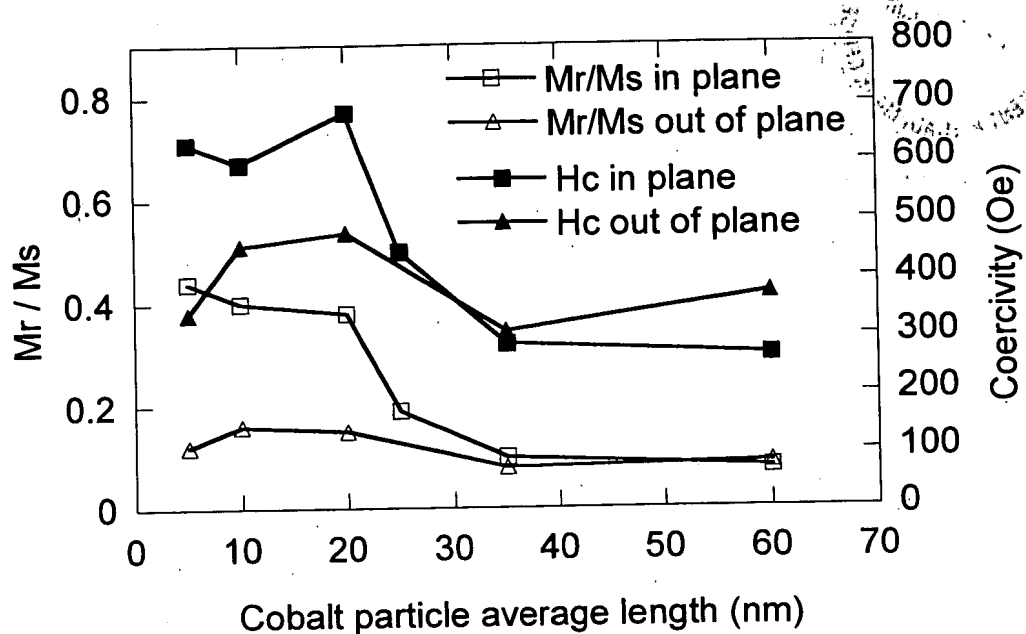


FIG. 11 Coercivity and Squareness vs. particle length of short Co particle arrays.

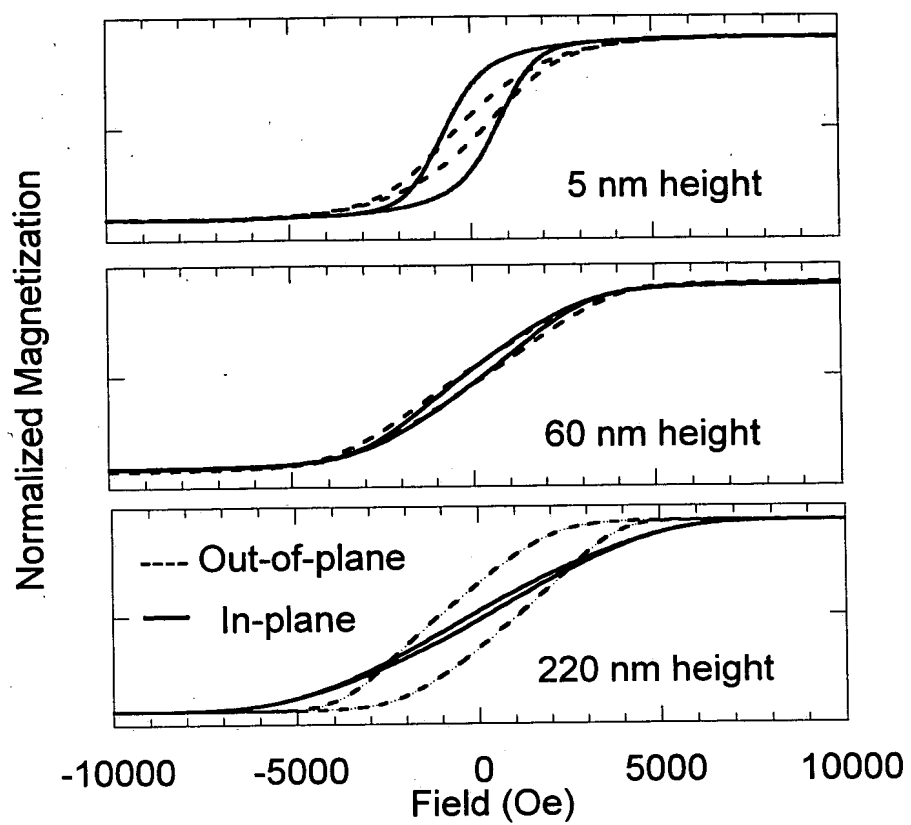


FIG. 12 Hysteresis loops of Co particle arrays with different thickness.

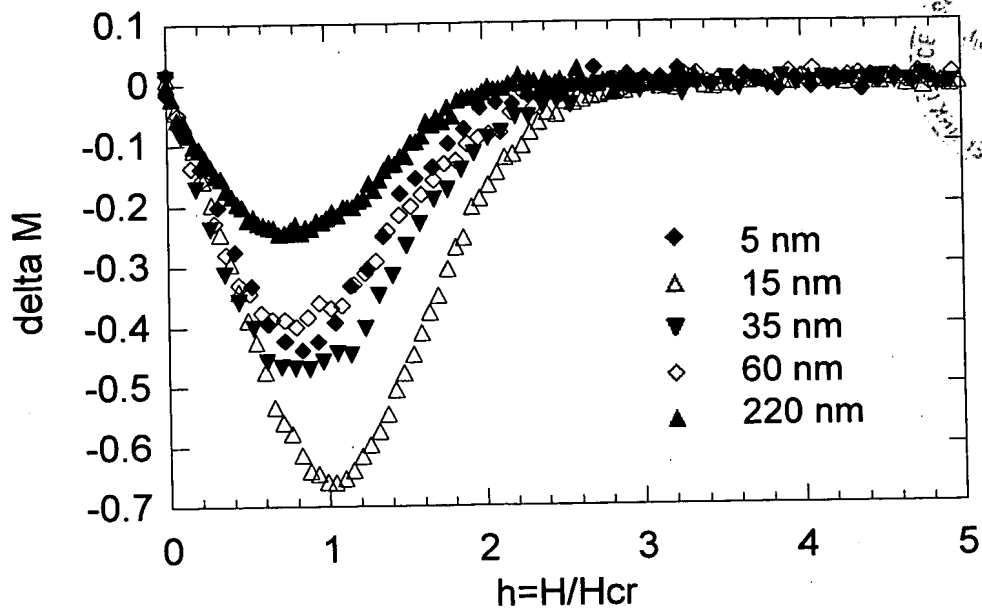
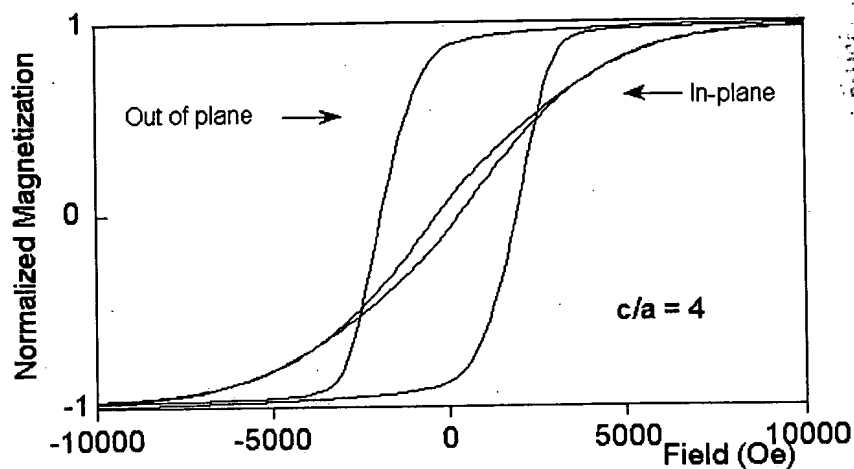
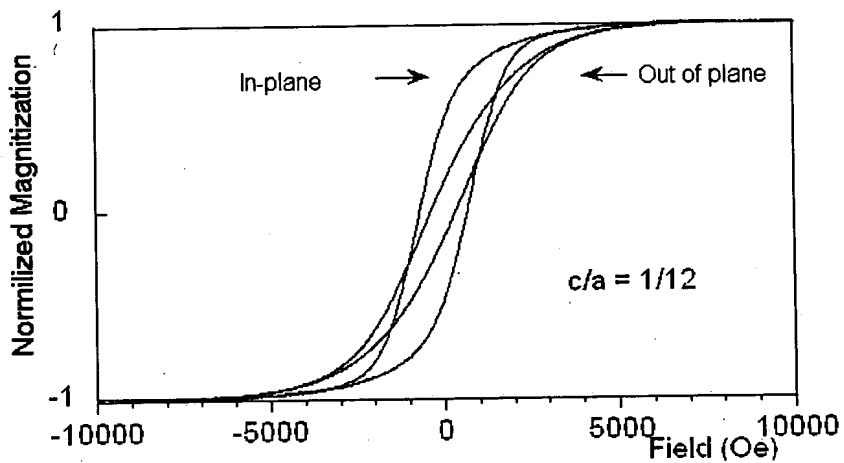


FIG. 13  $\Delta M$  curves vs. reduced applied field  $H/H_{cr}$  for various Co particle lengths.



5 Fig. 14 In-plane and out-of-plane hysteresis loops of  $l = 100$  nm Co nanoparticles, pore diameter  $d = 25$  nm [6], ratio  $c/a = 4$ . A sinusoidal waveform (Fig. 1a) was used for electrodeposition.



10 Fig. 15 In-plane and out-of-plane hysteresis loops of short Co nanoparticles obtained with an asymmetric rectangular waveform – length  $l = 5$  nm, pore diameter  $d = 60$  nm, ratio  $c/a = 1/12$ .